Key Engineering Materials
ISSN: 1662-9795, Vol. 926, pp 602-611
doi:10.4028/p-70x28i

Submitted: 2021-12-09
Revised: 2022-02-03
Accepted: 2022-02-03
Online: 2022-07-22

Effects of Tool-Workpiece Friction Condition on Energy Consumption during Piercing Phase of Seamless Tube Production

Hamed Aghajani Derazkola[1,a*], Eduardo Garcia[1,b], Alberto Murillo-Marrodán[1,c]

[1]Department of Mechanics, Design and Industrial Management, University of Deusto, 48007 Bilbao, Spain

[a]Hamed.aghajani@opendeusto.es, [b]e.garcia@deusto.es, [c]alberto.murillo@deusto.es

Keywords: hot piercing process, seamless tube, energy consumption, Super Cr13 steel, friction

Abstract. During the hot piercing phase of seamless tube production, friction and contact conditions between tools and workpiece significantly influence final product quality and energy consumption. The friction effects on the production of high alloyed steels like Super Cr13 steel are critical. This study analyses the effect of different friction conditions at the workpiece-tool interface in the piercing of Super Cr13 steel bars to minimize total energy consumption in such a manufacturing process. For this purpose, a three-dimensional finite element method (FEM) is employed to simulate and analyze the piercing process. The variety of tools (plug, rollers, and Diescher discs) and contact conditions lead to differences in the applied stress at different workpiece areas. Consequently, various friction models and friction coefficients were selected for different interfaces. The relation between strain rate, temperature, and geometry of pierced tube are discussed, and the selected friction relation with total power and energy consumption is presented. Experimental tests results have been used for evaluation of FEM output, and finally, the most effective conditions with lower total energy consumption are presented.

Introduction

One of the first stages during seamless tube manufacturing is the tube piercing phase (TPP). In this phase, a pre-cut billet with specific dimensions and geometry is heated up until its hot forming temperature for piercing [1]. The tooling system of the piercing process consists of two rollers and side guiding tools (rotational Diescher discs or static guiding shoes) that push the heated billet forward, and at the same time, a hard tool called plug starts to pierce billet with forwarding movement in the opposite direction of billet drive [2]. During TPP, rollers rotate with axes offset that is called feed angle. The prominent role of the roller is pushing forward the hot billet against the plug direction [3].

On the other hand, the side tool guides the billet and controls the dimension of the produced tube [4]. The forward movement produced by the rollers continues until the the billet is fully transformed into a hollow tube [5]. Tool shapes, feeding angle, and normal axis pressure are critical parameters for precise dimensions, defect-free, and good surface quality [6]. Among all parameters in this process, friction as a physical phenomenon at the interface of tools and workpiece plays the leading role [7]. The friction at a high temperature determines producibility and energy consumption during this process [8]. From a geometrical point of view, the friction occurs between rollers-workpiece, plug-workpiece, and guiding tool-workpiece interfaces [9]. From a manufacturing point of view, the friction between rollers and workpieces is the most important, because it is responsible for introducing power and movement into the system, and the contact area between rollers and billet is higher than other areas [10]. In this case, the piercing plug is freely rotating on its axis, and just the friction resistance in the piercing direction is important.

During TPP, the Diescher discs have rotational velocity, and the friction at the interface between discs and workpiece has little influence on workpiece advance but they are important for achieving the circular geometry of the product [11]. Consequently, the friction in this area does not have significant effects on materials flow compared to other tools. For the production of a sound tube, the driving friction on the roller-workpiece plus guides-workpiece should be balanced with the plug

friction condition. Owning to the complication of the TPP stage during the seamless tube production process, limited three-dimensional FEM studies have been published to understand thermo-mechanical phenomena between tooling system and workpiece. Also, the effects of friction conditions between the tooling system and super chromium steel on the total consumption energy at the TPP phase have not been considered. This article aims to study various friction conditions between the tooling system and super Cr13 steel to investigate energy consumption during the TPP phase.

Experiments

In this study, super Cr13 was selected as a base metal. Cr13 super martensitic stainless steel was used in the industrial process [12]. During the seamless tube production, the quality control section of the factory recorded the energy data. The chemical composition of selected steel is presented in Table 1.

Table 1. Chemical composition of 13Cr MSS

Element	C	Cr	Ni	Mn	Si	Mo	P	S	Ti	V	Fe
Wt.%	0.03	11.5-13.5	4.5-6.5	0.5	0.5	1.5-3	0.03	0.005	0.01-0.5	0.5	Bal

A casting factory made the super Cr13 shafts with the exact chemical composition presented in Table 1. A pice of super Cr13 with 840 mm length was cut from a casting shaft and used as a billet during tube piercing. At the first stage, the billet is heated up from ambient temperature (25ºC) until 1250ºC in a gas furnace. After that, the hot billet was transferred from furnace to the piercing section (Figure 1a). The hot billet slid into the chamber for positioning and became ready for next step.

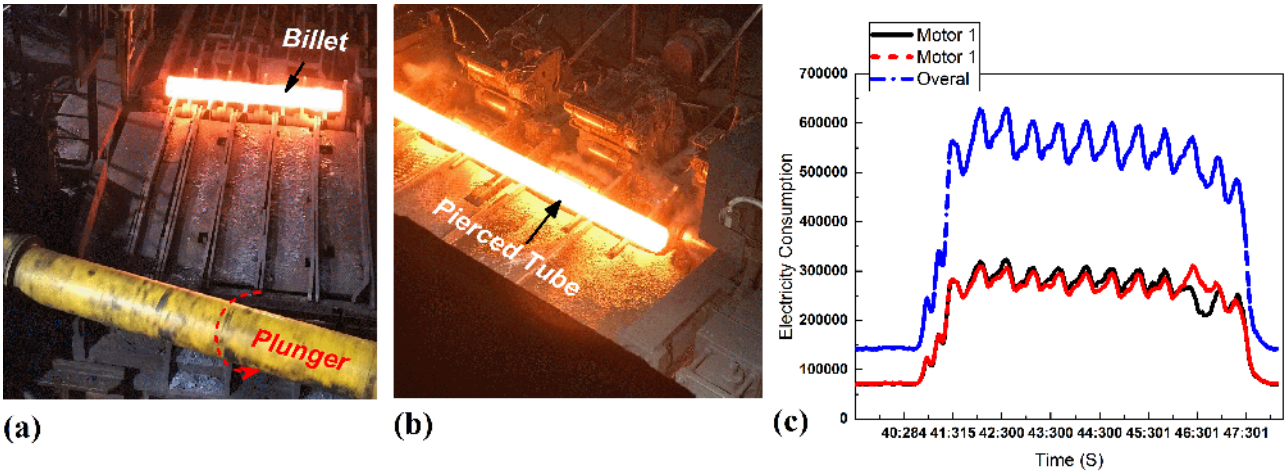

Figure 1. (a) Heating up of billet, (b) Pierced tube, (c) Recorded electricity usage of roller 1 (motor 1) and roller 2 (motor 2) during the piercing process.

In the chamber, a thrust bench pushes forward the hot billet into the main tooling box. The toling box consists of two rollers, a plug and two Diescher discs. The super Cr13 hot billet was pushed forward to pass through the plug (plug) with the axial force and contact friction of rollers. This involuntary movement caused that the plug pierced the billet. During the piercing, two Diescher discs control the geometry of the tube in order to limit the radial expansion of the hollow cavity. During piercing, the length of the billet is increased, and the thickness of tube walls is decreased. In this setup, the plug can rotate freely but is limited to moving in X, Y, or Z direction. At the end of this stage, the final tube is obtained (Figure 1b). The process parameters, geometrical issues, and wall thickness are not the aim of this study. For this reason, these points are ignored.

In order to validate the simulation experimental energy consumption is considered, especifically, the electricity consumption of the rollers which was recorded and converted representing the total power

consumption (Figure 3c). The experimental dimensions and kinematics of the tools and the billet are according to the details described in the simulation section.

Simulation

In this section, the preparing steps for simulation are described. At the early stage, the sketch of simulation domain of tube piercing phase was modeled in SolidWorks software. All parts were drawn separately and assembled in SolidWorks, and the assembly of the process was imported to Finite element software. The domain consists of two rollers, two Dieschers, a plug, a guide tube, a thrust bench, and a Cr13 MSS billet. The rollers had a 900 mm diameter with a 1.5° profile angle, 0° cross angle, and 12° feed angle. The assembly model from all parts is imported to the FORGE® NxT software. For simplicity of the simulation, all tools were selected as non-deformable (rigid) objects with thermal properties and billet-selected as deformable object with thermal properties—the tools were meshed by different sizes and a uniform mesh was set for the billet. The tools were meshed by 2D triangular elements, 0.7 size factor and 1 mm minimum size. The Cr13 steel billet was meshed by 3D tetrahedral P1+ linear elements with a bubble node, size factor of 0.7, volumic size factor of 2.2 and minimum 1.5mm mesh size. The length of the initial billet was selected at 840 mm. According to the experimental tests, the billet temperature was set 1250°C. The Isometric view of meshed sample and simulation domain in FORGE® NxT is presented in Figure 2a. The Hensel-Spittel constitutive law is chosen to model 13Cr MSS behavior at different temperatures, strain, and strain rates. The super Cr13 super martensitic sainless steel materials coeffiecient provided by industial company [13]. The flow stress curves obtained and with curve fitting approach, numbers and coefficient for Hansel-Spittel constitutive law were extracted and imported to the materials library of FORGE® NxT.

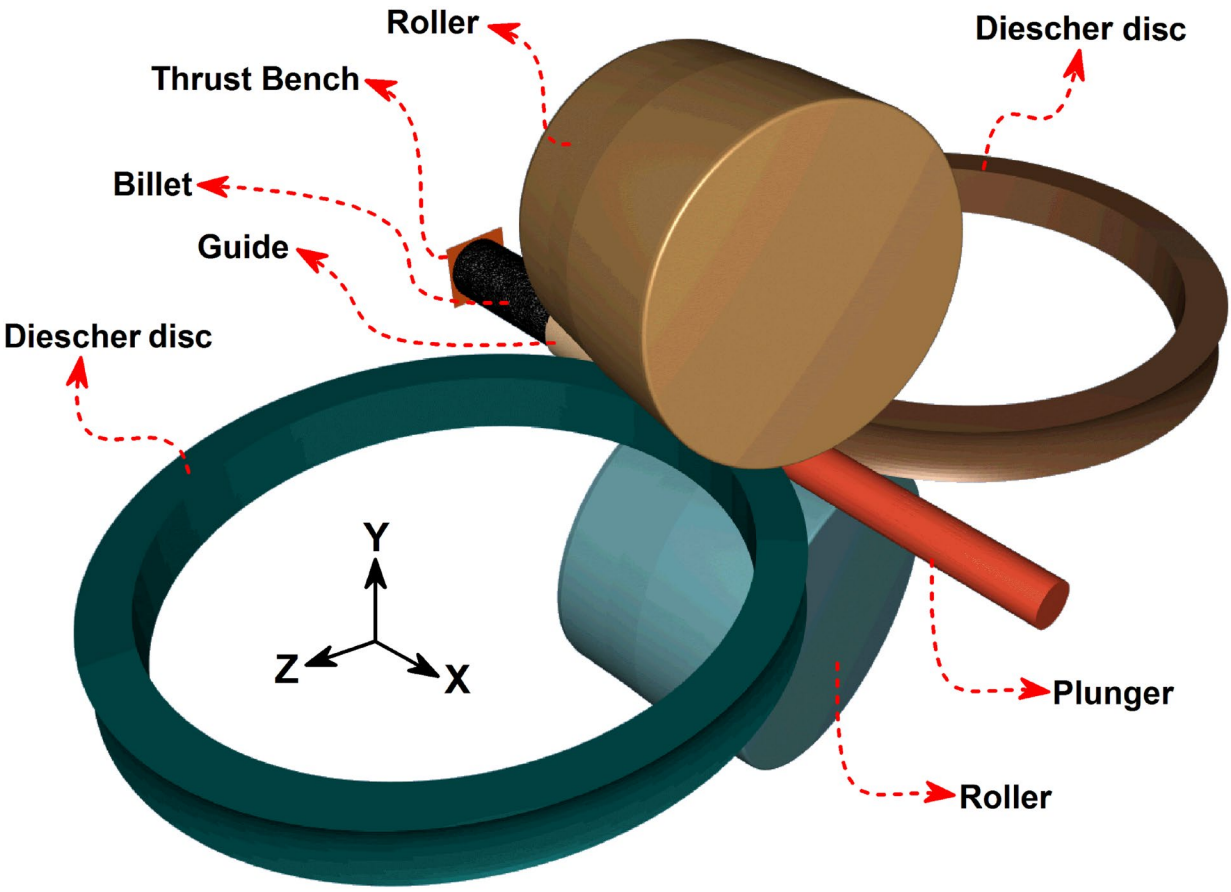

Figure 2. Isometric view of meshed billet and piercing tools.

During the Simulation section, the rollers and Dieschers were straight kept in touch with the billet. The contact between the Thrust bench and Guide with the billet were selected without friction. After the early stage of the piercing process, the billet pushed by the thrust bench and billet starts to contact

the plug. To better understand the contact situation between tools and billet, various friction models of Tresca, Viscoplastic, Neumaier, and IFUM were selected. Murillo-Marrodán et al. showed that during FEM simulation of TPP, the viscoplastic friction model at Roller-Billet interface has good agreement with experimental results and the Tresca friction model at other interfaces had good agreements with experimental outputs [14]. In this study, the various friction models for Roller-Billet (RF), Diescher-Roller (DF), and Plug-Billet (PF) interfaces were implemented. The best option for the RF interface was the viscoplastic model and the best friction model at DF and PF interfaces was the Tresca friction model. The selected friction models in this study had good agreements with real piercing test conditions and previous works of literature that considered friction conditions during TPP by the FEM method [15]. Finally, for a better understanding of friction conditions, different friction coefficients are selected for interfaces. The viscoplastic friction model for rollers and billet was selected, and the Tresca model was selected for other contact areas. With the aim of investigating the effects of friction coefficient, the discrete values between 0.1-0.5 were selected for the RF coefficient , PF coefficient selected between 0.06-0.15, and DF coefficient selected between 0.1-0.3. To better understand the effects of friction coefficient, a step-by-step plan was designed for selecting of friction coefficient presented in Table 2.

Table 2. Used friction models and friction coefficients at different interfaces

Interface	Roller-Billet	Diescher-Roller	Plug-Billet
Friction Model	Viscoplastic	Tresca	Tresca
Friction Coefficient	0.1	0.1	0.06
	0.2		
	0.3	0.2	0.1
	0.4		
	0.5	0.3	0.15

Results and Discussions

The bench pushes the hot billet during the tube piercing phase until the rollers contact the billet. Immediately after contact with rollers, the billet diameter start to reduce. The rollers pushed forward the billet until the middle of the tube contacted the plug. The plug pierced the moving billet. After that, the billet contact with the piercing plug, the piercing plug load grows, and the forward velocity of billet drops. The tube elongation and cross-section reduction starts after contacting the plug and helps to forward-moving the billet.

The primary role of Dieschers during the piercing phase is controlling the geometry. When the billet is contacted with all tools (rollers, plug, and Dieschers), the steady-state phase starts until the end of the process. Due to the higher contact areas of billet with rollers and plug, the frictional contacts in mentioned areas play prominent roles during the piercing process. On the other hand, due to the small contact area between Dieshers and billet, the effects of Dieshers on moving forward of the tube are not significant.

From the manufacturing point of view, it is essential that the piercing phase is finished correctly and the final sound tube produced. In this regard, the friction coefficient at interfaces plays the leading role in the quality of the final product and total energy consumption. Due to the selected friction coefficient between roller and workpieces, it is essential to check that all friction conditions conclude to produce a sound tube or not. In this regard, the simulation results revealed that the piercing process is not finished in 0.1 friction coefficient between roller and workpiece (Fig. 3a). It seems that with a low friction coefficient, the roller cannot push forward billet and overcome the resistance force of the plug. In this case, after contacting billet with rollers, the moving direction of billet stops and the pure sliding friction phenomena happens in the interfaces. Consequently, the sound tube is not produced in this situation.

By contrast, the results revealed that the final tube is formed at a roller friction coefficient above 0.1 (Fig. 3b). All samples with RF= 0.2, 0.3, 0.4, and 0.5 were pierced successfully. Friction values higher than 0.1 at the rollers-billet interface produce a forward force big enough to overcome plug

resistance force and finish the tube piercing phase. It seems, at a higher friction coefficient, the pure sliding friction condition convert to a sliding-sticking condition. The sticking condition kept the billet and pushed forward easier. This key factor helps to finish the piercing phase.

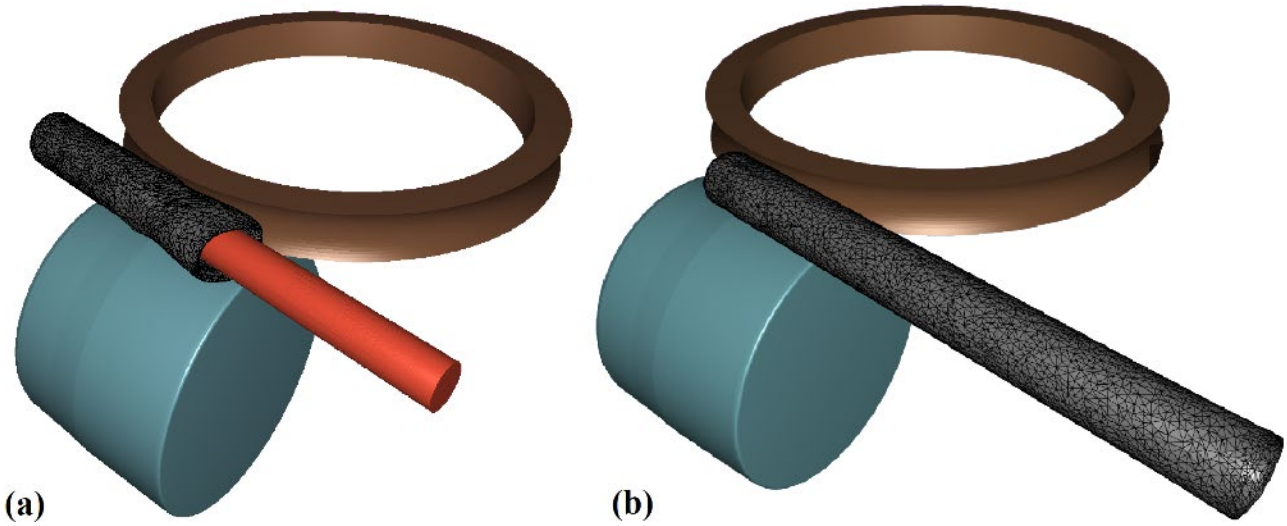

Figure 3. Simulation results of piercing phase at RF friction coefficient of (a) 0.1 and (b) 0.2.

As discussed before, the friction coefficient affects the frictional condition on the tools-billet interfaces. This factor also can be investigated by analysing the stress on the surface of the billet. The simulation results of Von Misses equivalent stress on the surface of Cr13 MSS billet at RF=0.1 and RF=0.2 are depicted in Fig. 4a and 4b, respectively. Due to the difference in the produced final tube, simulation results and the scale bar of FEM software are not the same. The simulation results at Fig. 4a, show that the stress distribution in the case of RF=0.1 is not symmetrical, and high stress values are distributed in the Cr13 MSS tube. The simulation results predicted that the maximum Von Misses equivalent stress was in contact areas of rollers and Diescher discs with billet. The difference between side stresses (that exert to the billet by Diescher discs) was not high comparing the stresses that applied by rollers on top and bottom of the billet. Due to available literature, the lateral sides stress applied by Diescher discs should be much lower than stresses applied by rollers in cases that the sound tube produced [1]. In the case of RF=0.1, the geometry of the tube head is formed elliptical shape. The tube must form hollow circular geometry, but in this case, the moving billet stopped after touching with rollers. After that, the tube expanded from the lateral sides. This phenomenon revealed that the flow of materials formed non-uniform [16]. In other words, the material flow at the billet's surface was faster than the internal. The rollers started to push forward the billet, but the friction factor at the interface of the rollers-billet was not enough to push the billet straight ahead and overcome the restriction force of the plug. The surface stress distribution was local and led to the flow of materials on the surface. The restriction forces of the plug stopped the pricing process while the rollers and Diescher discs were still rotating. Consequently, the surface stress by the Diescher disc increased. Increasing Diescher discs stress leads to faster materials flow in lateral sides, and the higher materials flow from sides leads to expansion of hot tube from lateral sides. For this reason, the stopped billet head formed an elliptical. With increasing RF, the applied forward force increased enough to finish the piercing process. The higher friction coefficient can overcome the plug restriction force and complete the pricing process [17]. The simulation results of RF=0.2 were depicted in Fig. 4b. As seen in Fig. 4b, the stress is applied locally on the interface of the roller-billet, and the distribution of stress is not comprehensive. The highest Von Mises equivalent stress in RF=0.2 was predicted in the rollers-billet interface, and on the other hand, the stress on Diescher discs is much lower than the rollers-billet interface. This phenomenon indicates that the rollers can push forward, and Diescher discs helps the forward-moving [18]. In this case, the flow of materials at the exterior and interior side of the tube is uniform, and for this reason, the geometry of produced tube was hollow circular.

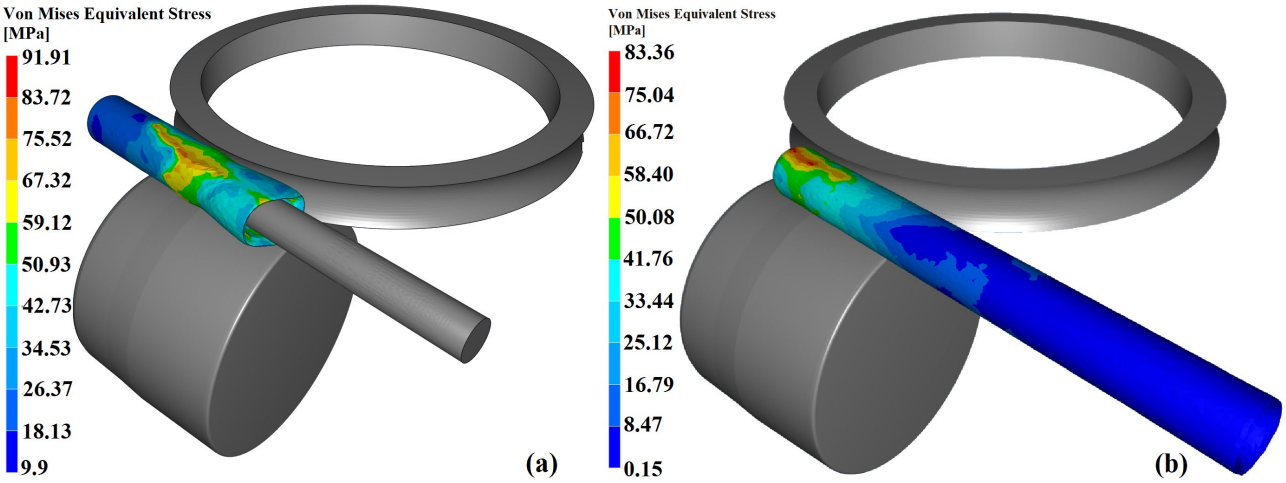

Figure 4. Simulation results of Von Misses equivalent stress on the Cr13 MSS billet at friction coefficient of (a) 0.1 and (b) 0.2.

After consideration, the production of the final tube, selecting the best option to minimize energy consumption could be a valuable effort. Due to selected parameters in this study, the produced tube in RF=02, 0.3, 0.4, and 0.5 was defect-free. In this way, it is necessary to find the minimum energy consumption during the tube piercing phase. The total power of all cases collected and the results reported and analysed. During the FEM simulation of this process, the total power of the piercing process is obtained by summation of the power dissipated by plastic deformation and power dissipated by friction. At the first step, the relation between the friction coefficient of rollers-billet interface with total power is considered. The simulation results of total power in RF=0.1 and RF=0.5 were ploted and presented in Figs. 5a and 5b, respectively. The simulation results clearly show that the total power increased from 1 second after thrust bench movements. From obtained results can be concluded that the billet contact with rollers and Diescher discs started after 1s. After that, the total power increased to a peak. This short time is the transforming period from starting piercing to a maximum amount of power. The transform period was not formed in the RF=0.1 case because the tube stuck, and the piercing process was not finished. In the RF=0.5 case, the transforming period was fast, and the steady-state phase started after that. In this phase, the billet is fully contacted with rollers, Diescher discs, and the plug. In other words, the full elongation and decreasing thickness start from the steady-state phase. After finishing the steady-state phase, the total power decreased indicated the final stage of the piercing process. The simulation results revealed that the total power of the piercing phase in RF=0.1 is much higher than in other cases. As expected, the sliding friction condition and uncompleted tube increased the energy consumption in this case. There is a big difference between friction power and plastic deformation power in RF=0.1, and the total power is near to plastic deformation power. This result indicated that the frictional power was not enough to finish the process, and the total power was wasted for the whole process.

With increasing frictional coefficient, the plastic power increased and caused to increase in total power. The collected simulation data made it clear that the total power with increasing friction coefficient grows (Fig. 5c). On the other hand, the experimental results have good agreements with the RF=0.2 case. According to obtained results, the frictional power decreased by increasing RF, and the plastic deformation power increased. This phenomenon is affected by process time (Fig. 5d). The results show that with increasing RF, the processing time decreases, and consequently, the plastic deformation power increases. As a consequence, it can be found that with increasing plastic deformation and decreasing process time, the strain rate of Cr13 MSS increased by increasing RF. The obtained results revealed that the total power or RF=0.2 from ~5250kW increased to ~7000kW in RF=0.5. From RF=0.2 until RF=0.5, the frictional power decreased from 1800kW to 1400kW, while the plastic power increased ~3450kW to ~5600kW. On the other hand, the total time for the piercing process in RF=0.2 from 4.3s decreased to 2.6s in RF= 0.5. These numbers revealed that the friction coefficient determines the total time of process and Cr13 billet strain rate.

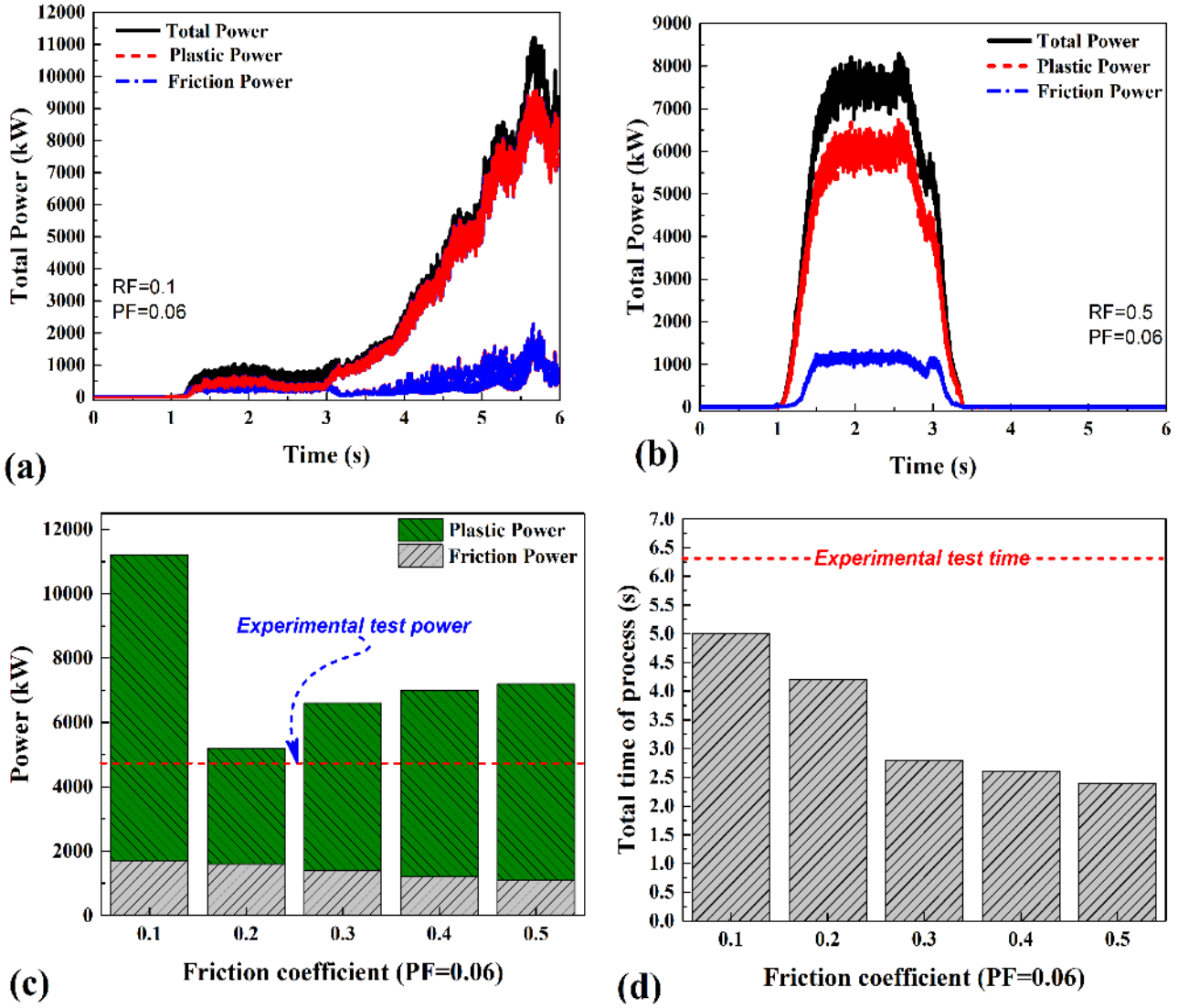

Figure 5. Simulation results of total power in (a) RF=0.1 and (b) RF=0.5. (c) Comparison between total power and various friction coefficient of rollers-billet interfaces. (d) Comparison between piercing process time and various friction coefficients of rollers-billet interfaces.

For a better understanding of friction coefficient effects on other interfaces, the friction coefficient at the plug-billet interface was investigated. Because the results of RF=0.2 had good agreements with the experimental test, this RF was selected for further study. In this regard, PF=0.06, PF=0.1, and PF=0.15 were selected and examined. The PF=0.06 and RF=0.15 results of total power from the simulation are presented in Figs. 6a and 6b, respectively. The obtained results indicated that with increasing plug friction, the total power of the piercing process decreases. This decrease is related to diminish of plastic power and friction power. The statistical analysis of all PFs is presented in Fig. 6c. Simulation results revealed that both friction power and plastic power decreased by increasing the friction coefficient in the plug-billet interface. In fact, with increasing plug friction, the total time of the piercing process increases, and consequently, the stain rate of the process decreases. The results of PF effects on process time are presented in Fig. 6d. It can be concluded that the more resistance formed by a higher plug friction coefficient, the less plastic deformation power. The results indicated that the higher friction coefficient at the interface of Dieschers does not significantly affect the total power of the process.

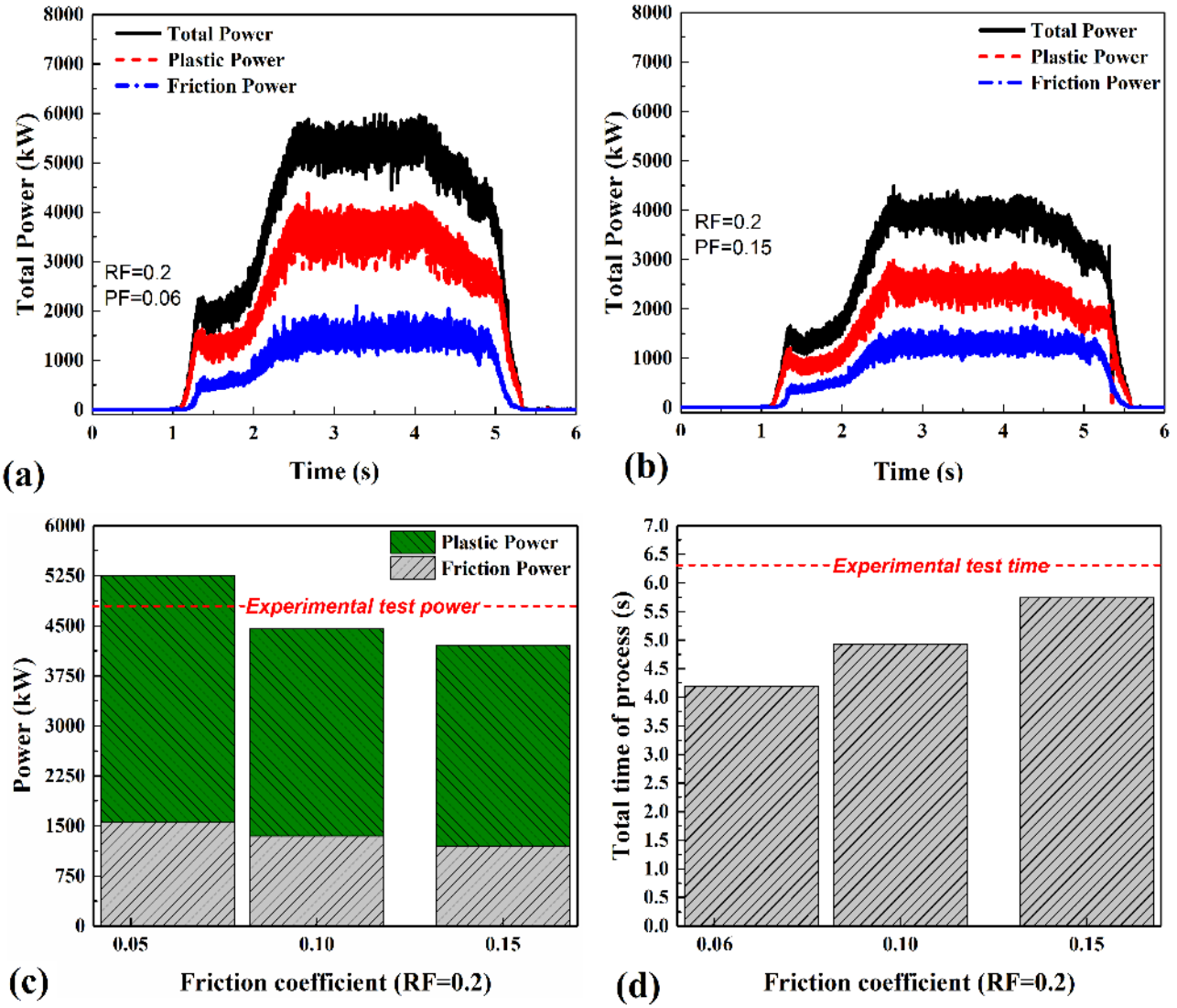

Figure 6. Simulation results of total power in RF=0.2 and (a) PF=0.06 and PF=0.15. The statically results of PF and total power. (d) The statically results of PF and process time.

Conclusion

This article has established a 3D finite element simulation of the Cr13 MSS tube piercing process. Different Friction models have been selected to the tools-billet interfaces and effects of friction coefficient for the different interfaces investigated. The results show that the friction coefficient at the RF interface can affect the quality of produced tube, strain rate of base metal, and stress distribution in Cr13 MSS billet during piercing. Diescher disc friction helps forward-moving billet during piercing, and the plug friction can increase the piercing process time. The total power of the piercing process increases by increasing the RF interface friction coefficient. At a higher friction coefficient of the plug-billet interface, the plastic deformation power decreases, and the total power of the piercing process decreases moderately.

Acknowledgments

This project has received funding from the European Union's Horizon 2020 Research and Innovation Programme under the Marie Skłodowska-Curie grant agreement No. 847624. In addition, a number of institutions back and co-finance this project.

References

[1] Brensing, K.-H.; Großrohre, S. Steel Tube and Pipe Manufacturing Processes.; 2004.

[2] Murillo-Marrodán, A.; García, E.; Barco, J.; Cortés, F. Analysis of Wall Thickness Eccentricity in the Rotary Tube Piercing Process Using a Strain Correlated FE Model. *Met.* 2020, *10*.

[3] Murillo-Marrodán, A.; García, E.; Barco, J.; Cortés, F. Application of an Incremental Constitutive Model for the FE Analysis of Material Dynamic Restoration in the Rotary Tube Piercing Process. *Mater.* 2020, *13*.

[4] Zhang, Z.; Liu, D.; Yang, Y.; Zheng, Y.; Pang, Y.; Wang, J.; Wang, H. Explorative study of rotary tube piercing process for producing titanium alloy thick-walled tubes with bi-modal microstructure. *Arch. Civ. Mech. Eng.* **2018**, *18*, 1451–1463, doi:https://doi.org/10.1016/j.acme.2018.05.005.

[5] Nikitin, M. V; Maslyuk, V.M.; Lazko, N. V Improving the wear resistance of structural steels through the use of metallurgical production factors. *Metallurgist* **2010**, *54*, 28–32, doi:10.1007/s11015-010-9249-6.

[6] Skripalenko, M.M.; Bazhenov, V.E.; Romantsev, B.A.; Skripalenko, M.N.; Huy, T.B.; Gladkov, Y.A. Mannesmann piercing of ingots by plugs of different shapes. *Mater. Sci. Technol.* **2016**, *32*, 1712–1720, doi:10.1080/02670836.2016.1145840.

[7] solving contact problems in metal forming simulation. *Int. J. Numer. Methods Eng.* **1999**, *46*, 1435–1462, doi:https://doi.org/10.1002/(SICI)1097-0207(19991130)46:9<1435::AID-NME707>3.0.CO;2-9.

[8] Chastel, Y.; Diop, A.; Fanini, S.; Bouchard, P.O.; Mocellin, K. Finite Element Modeling of Tube Piercing and Creation of a Crack. *Int. J. Mater. Form.* **2008**, *1*, 355–358, doi:10.1007/s12289-008-0068-2.

[9] Ceretti, E.; Giardini, C.; Brisotto, F. 2D Simulation and Validation of Rotary Tube Piercing Process. *AIP Conf. Proc.* **2004**, *712*, 1154–1159, doi:10.1063/1.1766684.

[10] Topa, A.; Kim, D.K.; Kim, Y. 3D Numerical Simulation of Seamless Pipe Piercing Process by Fluid-Structure Interaction Method. *MATEC Web Conf.* **2018**, *203*.

[11] Fernandes, M.; Marouf, N.; Montmitonnet, P.; Mocellin, K. Impact of the Different Friction Coefficients on the Tools on the Mechanics of the Mannesmann 2-roll Tube Piercing. *ISIJ Int.* **2020**, *60*, 2917–2926, doi:10.2355/isijinternational.ISIJINT-2020-290.

[12] Derazkola, H.A.; García Gil, E.; Murillo-Marrodán, A.; Méresse, D. Review on Dynamic Recrystallization of Martensitic Stainless Steels during Hot Deformation: Part I—Experimental Study. *Met.* 2021, *11*.

[13] No Title Available online: https://www.tubosreunidos.com/.

[14] Murillo-Marrodán, A.; García, E.; Cortés, F. A Study of Friction Model Performance in a Skew Rolling Process Numerical Simulation. *Int. J. Simul. Model.* **2018**.

[15] Murillo-Marrodán, A.; García, E.; Cortés, F. Modelling of the cone-type rotary piercing process and analysis of the seamless tube longitudinal shear strain using industrial data. *AIP Conf. Proc.* **2019**, *2113*, 40003, doi:10.1063/1.5112537.

[16] Ghiotti, A.; Fanini, S.; Bruschi, S.; Bariani, P.F. Modelling of the Mannesmann effect. *CIRP Ann.* **2009**, *58*, 255–258, doi:https://doi.org/10.1016/j.cirp.2009.03.099.

[17] Komori, K. Simulation of Mannesmann piercing process by the three-dimensional rigid-plastic finite-element method. *Int. J. Mech. Sci.* **2005**, *47*, 1838–1853, doi:https://doi.org/10.1016/j.ijmecsci.2005.07.009.

[18] Romantsev, B.A.; Skripalenko, M.M.; Huy, T.B.; Skripalenko, M.N.; Gladkov, Y.A.; Gartvig, A.A. Computer Simulation of Piercing in a Four-High Screw Rolling Mill. *Metallurgist* **2018**, *61*, 729–735, doi:10.1007/s11015-018-0556-7.